Simulations of terrestrial carbon metabolism and atmospheric CO$_2$ in a general circulation model

Part 1: Surface carbon fluxes

By A. SCOTT DENNING[1]*, G. JAMES COLLATZ[2], CHANGAN ZHANG[3], DAVID A. RANDALL[3], JOSEPH A. BERRY[4], PIERS J. SELLERS[2], GREG D. COLELLO[4] AND DONALD A. DAZLICH[3], [1]*School of Environmental Science and Management, University of California, Santa Barbara, CA 93106-5131, USA;* [2]*National Aeronautic and Space Administration, Goddard Space Flight Center, MS 923, Greenbelt, MD 20771, USA;* [3]*Department of Atmospheric Science, Colorado State University, Fort Collins, CO 80521–371, USA;* [4]*Carnegie Institute of Washington, Department of Plant Biology, Stanford, CA 94305, USA*

ABSTRACT

The exchange of carbon dioxide (CO$_2$) between the atmosphere and terrestrial ecosystems due to photosynthesis and respiration has been simulated using a new version of the simple biosphere model (SiB2) and the Colorado State University (CSU) general circulation model (GCM). Parameters associated with the extent and seasonality of vegetation were derived from satellite observations. The fluxes were calculated at the GCM time step of 6 min, so that the diurnal cycle of photosynthesis is well resolved. Annual net primary productivity simulated by the coupled model agrees well with previous estimates in most regions of the world. In some regions (central North America, southeastern South America, southeast Asia), the precipitation simulated by the CSU GCM is less than observed, and in those regions the simulated NPP is less than previous estimates. The amplitude of the seasonal cycle of the simulated net flux is quite similar to previous estimates, but the phase is significantly earlier in the northern temperate and boreal zones, both as simulated by the GCM and when SiB2 is driven off-line using observed meteorological forcing. At the few locations for which observational data are available, the phase of the simulated seasonal cycle of net carbon fluxes agrees well with the data, but at one temperate forest grid cell the amplitude is too low. The phase of the simulated diurnal cycle reproduces observations from a temperate forest, temperate grassland, and tropical forest. The amplitude of the simulated diurnal cycle is close to the observed amplitude early in the season at the temperate grassland site, but deteriorates by late summer because of drought stress due to the less-than-observed simulated precipitation.

1. Introduction

On time scales of minutes to months, the concentration of atmospheric CO$_2$ is modulated by terrestrial photosynthesis and respiration, accounting for most of the seasonal and diurnal variability of atmospheric CO$_2$ around the world (Keeling, 1958; Hall et al., 1975; Fung et al., 1983, 1987; Keeling et al., 1989a; Heimann et al., 1989). Annual one-way fluxes from these two processes exceed anthropogenic CO$_2$ emissions by more than an order of magnitude, but uptake and release of CO$_2$ are largely balanced at the global scale (Schimel et al., 1995). It has been suggested that carbon has been accumulating in terrestrial ecosystems in recent decades due to an imbalance

---

* Corresponding author.

between photosynthetic uptake and respiratory efflux resulting from direct fertilization by anthropogenic CO_2 (Gifford, 1994), nutrient deposition (Schindler and Bayley, 1993), reforestation (Dixon et al., 1994), climate change (Dai and Fung, 1993), or some combination of these factors. Such a sink may account for more than half of the CO_2 released by fossil fuel combustion (Francey et al., 1995), but would amount to less than 5% of annual carbon uptake by photosynthesis, which is well within the range of uncertainty of current estimates.

Interactions between the Earth's climate and carbon cycle are complex and interwoven: CO_2 affects the radiative balance of the atmosphere (Shine et al., 1995) and therefore the climate, and through the mechanisms outlined above can change global and regional patterns of carbon sources and sinks. The state of the Earth's climate and biosphere a few centuries hence will depend on a *coupled* response of the atmosphere-biosphere system to rising CO_2 concentrations, and investigations which arbitrarily treat either the climate or the surface carbon exchanges as the "forcing" and the other as the "response" are unlikely to prove really useful in predicting long term change.

Direct measurement of atmosphere-biosphere exchange of CO_2 at the ecosystem level is difficult and expensive, but long-term data sets from eddy correlation studies are finally becoming available (Shuttleworth et al., 1991; Wofsy et al., 1993; Sellers et al., 1995). Although such field data are invaluable for understanding the behavior of natural ecosystems, they represent small spatial scales, and integration of these measurements to the global scale is not possible at this time. Furthermore, field experiments cannot be used to predict how terrestrial carbon fluxes might change due to changes in climate and atmospheric composition.

Estimates of terrestrial carbon exchange used to drive global models have long been made by applying statistical relationships between field measurements and climate parameters such as precipitation and temperature to gridded climatological data sets, combined with maps of land-cover types and remotely sensed data (Lieth, 1975; Fung et al., 1983). Seasonal variations of surface carbon exchange have been calculated by combining these statistical relationships with satellite data (Fung et al., 1987; Heimann and Keeling, 1989;

Friedlingstein, 1994, 1995; Foley 1994; Maisongrande et al., 1995). In recent years, simulations of seasonal carbon metabolism on the global scale have also been performed using more physiologically based ecosystem models forced by observed climatology (Raich et al., 1991; Melillo et al., 1993) and remotely sensed data (Potter et al., 1993). These models are computationally efficient enough to allow for very long integrations (hundreds or thousands of years), so they can be allowed to develop organic carbon pools in equilibrium with the prescribed climate. Unfortunately, they generally use monthly time steps, which means they cannot be used to simulate nonlinear interactions between fluxes and transport at shorter time scales.

Bonan (1995) performed a coupled simulation of climate and carbon flux at the land surface using the Community Climate Model (CCM) at the National Center for Atmospheric Research (NCAR). His approach had the advantage of a short time step which resolved seasonal, synoptic, and diurnal variations in carbon metabolism, and his global fields of annual net primary production (NPP) agreed fairly well with previously published estimates using ecosystem models. Furthermore, by performing the calculation inside the CCM, his model allowed interactions between the simulated climate and carbon fluxes via the surface energy budget at the land surface. Because carbon assimilation and respiration were parameterized independently, strong net sources and sinks were obtained over large regions, with the land surface acting as a global net sink of about 5 Gt C yr^{-1} over the 5 years of his integration.

In this paper, we present the results of a simulation of terrestrial carbon metabolism with a coupled model of climate and terrestrial physiology and biophysics. The land-surface processes (including carbon fluxes) are simulated using a new version of the simple biosphere model of Sellers et al. (1986), which has been substantially revised and is now referred to as SiB2 (Sellers et al., 1996a,b; Randall et al., 1996). SiB2 runs within the Colorado State University (CSU) General Circulation Model (GCM). Like the study of Bonan et al. (1995), we calculate the carbon fluxes interactively with the climate simulation at a short time step that resolves important nonlinear interactions that may affect the annual mean distribution of CO_2. Unlike the previous study,

however, the simulated release of carbon by respiration is constrained by the previous year's gross photosynthesis, which isolates the effect of the "neutral" terrestrial biosphere on the spatial distribution of atmospheric CO_2.

Both the CSU GCM and SiB2 are described in Section 2. In Section 3, we consider the simulated carbon metabolism on the global scale and the influence of departures of the simulated from the observed climate. In Section 4, we evaluate the realism of the simulated seasonal and diurnal cycles of the carbon fluxes at specific grid points for which observational data are available for comparison. Section 5 summarizes our results. We have also simulated the effect of the land surface fluxes presented here on the mixing ratio of atmospheric CO_2 with atmospheric transport calculated in the GCM. In a companion paper (Denning et al., hereafter referred to as "Part 2"), we present our results for the simulated concentration fields and atmospheric transport in terms of the diurnal and seasonal cycles and annual means, and compare these to observational data.

2. Model description

2.1. The CSU GCM

The CSU GCM is derived from the UCLA GCM, which was developed at UCLA, over a period of 20 years, by Professor A. Arakawa and collaborators. A copy of the model was brought to the Goddard Laboratory for Atmospheres in 1982, and from there to CSU in 1988. Many changes have been made since the model left UCLA, including revised parameterizations of solar and terrestrial radiation (Harshvardhan et al, 1987), the planetary boundary layer (PBL) (Randall et al., 1992), cumulus convection (Randall and Pan, 1993), cloud microphysical processes (Fowler et al., 1996), and land-surface processes (Sellers et al., 1986, 1989, 1992*a*, *c*, 1996*a*, *b*). Some recent results are presented by Randall et al. (1989, 1991, 1996), Stephens et al. (1993), Fowler et al. (1996), and Fowler and Randall (1996*a*, *b*).

The prognostic variables of the CSU GCM are: potential temperature; the horizontal wind components; the surface pressure; the PBL depth and turbulence kinetic energy; the mixing ratio of three phases of water plus rain and snow; the temper-

atures of the plant canopy, the ground surface, and the deep soil; the water contents of four above-ground and three below-ground moisture stores; the stomatal conductance of the plant canopy; and the ice temperature at land ice and sea ice points. The governing equations are finite-differenced, using highly conservative schemes (Arakawa and Lamb, 1977, 1981). Fourier filtering of the mass flux and pressure gradient vectors is used to maintain computational stability near the poles (Arakawa and Lamb, 1977).

A key feature of the GCM is its formulation in terms of a modified sigma coordinate, in which the PBL top is a coordinate surface, and the PBL itself is identified with the lowest model layer (Suarez et al., 1983). The mass sources and sinks for the PBL consist of large-scale convergence or divergence, turbulent entrainment, and the cumulus mass flux. Turbulent entrainment can be driven by positive buoyancy fluxes, or by shear of the mean wind in the surface layer or at the PBL top.

The cumulus mass flux and the warming and drying of the free atmosphere due to cumulus convection are determined through the cumulus parameterization of Arakawa and Schubert (1974; see also Lord et al., 1982), as modified by Randall and Pan (1993). Quasiequilibrium of the cloud work function is closely approximated through the use of a prognostic cumulus kinetic energy. The ice phase is taken into account in the cumulus parameterization. Cumulus friction is included, assuming momentum conservation in the convective updrafts. The effects of convective downdrafts are not currently included.

Stratiform clouds and precipitation are simulated by a new parameterization (EAULIQ) of liquid and ice cloud microphysics (Fowler et al., 1996). Five prognostic variables are used to track the mixing ratios of water vapor, cloud water, cloud ice, and falling rain and snow in the model, with transformation between phases representing condensation, freezing, melting, ice deposition, evaporation, sublimation, and mixed-phase physical processes. Large-scale saturation at the grid scale can lead to formation of cloud water and ice, and the cumulus parameterization also provides detrained water and ice as inputs to EAULIQ. In order to allow microphysical transformations among the five phases of water substance simulated in the model, rain and snow

particles do not fall instantly to the ground but rather are time-stepped explicitly, with collection, evaporation, melting, and freezing occurring during their descent. Optical and infrared radiative properties of the clouds are parameterized according to the cloud water, cloud ice, and snow paths. No clouds may form in the model above the 100 mb level, and no parameterization of fractional cloudiness is used in the free troposphere.

The radiation parameterization of the model is that of Harshvardhan et al. (1987). The terrestrial radiation parameterization includes cooling due to water vapor, carbon dioxide, and ozone. The solar radiation parameterization includes Rayleigh scattering and absorption by water vapor and ozone, and simulates both the diurnal and seasonal cycles. A complete (solar and terrestrial) radiation calculation is done once per simulated hour, in order to resolve adequately the diurnal cycle and the effects of transient cloudiness. A zonally uniform ozone distribution is prescribed as a function of latitude, height, and season.

2.2. The simple biosphere model (SiB2)

For vegetated land points, the surface fluxes of sensible and latent heat, radiation, moisture, and momentum are determined using the Simple Biosphere (SiB) parameterization developed by Sellers et al. (1986). SiB has recently undergone substantial modification (Sellers et al., 1996a, c; Randall et al., 1996), and is now referred to as SiB2. The number of biome-specific parameters has been reduced, and most are now derived directly from processed satellite data rather than prescribed from the literature. The vegetation canopy has been reduced to a single layer. Another major change is in the parameterization of stomatal and canopy conductance (Collatz et al., 1991, 1992; Sellers et al., 1992a, c, 1996a) used in the calculation of the surface energy budget over land. This parameterization involves the direct calculation of the rate of carbon assimilation by photosynthesis, making possible the calculation of CO_2 exchange between the atmosphere and the terrestrial biota at the dynamic time step of the CSU GCM.

Following Collatz et al. (1991, 1992) and Ball (1988), stomatal conductance, the carbon assimilation rate, and the CO_2 concentration at the leaf surfaces are assumed to be related by

$$g_s = m \frac{A_n h_s}{C_s} p + b, \qquad (1)$$

where g_s is the stomatal conductance to water vapor, A_n is the net assimilation rate of CO_2, h_s and C_s are the relative humidity and partial pressure of CO_2 at the leaf surface, respectively, p is the atmospheric surface pressure, and m and b are empirically-derived parameters.

The net assimilation rate A_n is modeled as limited by the kinetics of the carboxylation enzyme rubisco (Farquhar et al., 1980), by the conversion of light energy to chemical energy, and by the utilization of the sugars and starches that are the end products of photosynthesis. Collatz et al. (1991) defined the three limitations as follows: ω_c is the carbon-limited rate of photosynthesis (often referred to as rubisco-limited, since the rate is determined by rubisco enzyme kinetics), ω_e the rate limited by electron transport (light-limited), ω_s is the end product-limited (or sink-limited) rate. R_l is the rate of carbon loss due to leaf respiration. Farquhar et al. (1980) used a simple minimum of the three limits to calculate the assimilation rate

$$A_n = \min(\omega_c, \omega_e, \omega_s) - R_l; \qquad (2)$$

SiB2 uses a similar approach, but replaces the simple minimum in (2) with a smoothed function (Collatz et al., 1991) to avoid abrupt transitions from one limitation to another.

The rubisco-limited and light-limited assimilation rates are calculated from enzyme kinetics for C_3 (Collatz et al., 1991) and C_4 (Collatz et al., 1992) physiologies. The sink-limited rate is parameterized simply as a fraction of the maximum rubisco activity for C_3 vegetation, and reflects the activity of the enzyme PEP-carboxylase for C_4 vegetation. Leaf respiration R_l is parameterized according to maximum rubisco activity and canopy temperature.

Partial pressures of CO_2 are calculated in the canopy air space (C_a), at the leaf surface (C_s), and in the leaf interior (C_i), according to

$$A_n = \frac{g_s}{1.6} \frac{(C_s - C_i)}{P} = \frac{g_b}{1.4} \frac{(C_a - C_s)}{P} \qquad (3)$$

where g_b is the aerodynamic resistance across the leaf boundary layer. In the C_3 model, ω_c and ω_e respond to C_i, whereas in the C_4 model, only ω_s is sensitive to CO_2.

The stomatal conductance controls A_n mainly by limiting C_i (Sellers et al., 1996a), according to

$$C_i = C_s - \frac{1.6 A_n}{g_s} p. \tag{4}$$

Collatz et al. (1991) used an iterative procedure to simultaneously solve (2), (3), and (4) for g_s, A_n, and C_i. For computational efficiency in the GCM, g_s is updated as a prognostic variable in SiB2, using a scheme which relaxes the new value of g_s toward that predicted from (1), while using the "old" value to calculate A_n and C_i (see Sellers et al., 1996a).

All 3 photosynthetic limitations and the leaf respiration are scaled by nondimensional parameters (f_{hot}, f_{cold}, and f_ψ) representing environmental stresses due to excessively high or low canopy temperature and drought, and the stomatal conductance formulation includes a stress function that treats the influence of frozen soil. The leaf-level assimilation rate, stomatal conductance, and other physiological parameters are scaled to the canopy using a hypothesized optimal relationship between leaf nitrogen (and hence rubisco) and the time-mean profile of photosynthetically active radiation in the canopy. Details of the parameterization are presented by Sellers et al. (1996a, Appendix C).

2.3. Diagnostic calculation of soil respiration

The net exchange of CO_2 between terrestrial ecosystems and the atmosphere is defined as the net ecosystem exchange (NEE), and is calculated as

$$NEE = R - A_c \tag{5}$$

where R is the release of CO_2 from soils due to respiration (including respiration by both plant roots and soil microbes) and A_c is the integrated canopy net assimilation due to photosynthesis. In order to evaluate the surface carbon budget, we need to determine the respiration rate. SiB2 does not currently include a parameterization of soil respiration, although one is under development. In the present study, we use a simple diagnostic method to determine the soil respiration rate.

The relative intensity of soil respiration, denoted by R^*, is diagnosed from soil moisture and soil temperature at each model time step following the method used by Raich et al. (1991) in the

Terrestrial Ecosystem Model. The soil respiration diagnostic, R^*, is defined as

$$R^* = 2.0^{Q_t} f(M), \tag{6}$$

where

$$Q_t = (T - 298)/10, \tag{7}$$

and

$$f(M) = 0.2 + w_{sat}^B,$$

$$B = \left[\frac{w^{z_m} - w_{opt}^{z_m}}{w_{opt}^{z_m} - 100^{z_m}} \right]^2. \tag{8}$$

The temperature used to define Q_t in (7) is the warmer of the surface soil temperature and the deep soil temperature. The variable w in (8) is the fraction of the pore space occupied by water in the root zone (middle layer) of the soil. The parameters w_{sat}, w_{opt}, and z_m are prescribed according to soil texture using values suggested by Raich et al. (1991). Soil respiration is a maximum for some value w_{opt} of soil moisture, and respiration is less under very dry or very wet conditions.

A dimensionless monthly mean soil respiration rate is defined as

$$\bar{r}(t) = \frac{\bar{R}^*(t)}{\sum_{1 \text{ year}} \bar{R}^*(t) \, \Delta t}, \tag{9}$$

where the overbar indicates the monthly mean. The flux of CO_2 from the soil due to respiration is computed from this dimensionless rate as

$$\bar{R}(t) = \bar{r}(t) \sum_{1 \text{ year}} \bar{A}_C(t) \, \Delta t. \tag{10}$$

Eq. (10) represents the assumption of a local steady state for carbon storage in terrestrial ecosystems on an annual basis, i.e., that the annual sum of respiration loss is equal to the annual sum of the canopy net carbon assimilation, so that the net annual flux of CO_2 from every grid point is zero.

We recognize that the constraint of annually balanced carbon fluxes results in some loss of generality. Our method is unsuited to the direct calculation of net sources and sinks at the land surface, for example. Ecosystem respiration depends to first order on the inventory of carbon in various "pools" (wood, litter, roots, soil organic matter, etc.), the sizes of which are only known at a very few locations (Potter et al., 1993). Attempts

to simulate ecosystem carbon fluxes due to photosynthesis and respiration independently of one another are extremely sensitive to the initial sizes chosen for each pool at each model grid point. If the carbon pools are initialized by extrapolation from literature values in such a way that they are not in equilibrium with the simulated climate and NPP, large local and regional net imbalances will result at the annual time scale (Bonan, 1995). Such imbalances are transient responses to the initial conditions (soil carbon pools), and such a model may not reach equilibrium for many decades because of the slow turnover times of the more recalcitrant carbon pools.

To avoid this problem, we separate the atmosphere-biosphere exchange of carbon into the purely seasonal component represented here and a net annual source or sink, which can be parameterized separately (see Denning, 1994) and scaled by inversion of atmospheric data (Tans et al., 1989; Enting and Mansbridge, 1989, 1991; Keeling et al., 1989b; Tans et al., 1990; Enting et al., 1995). This approach allows the annual mean behavior of the biosphere to be constrained by the atmospheric observations, which are less uncertain than the calculated respiration fluxes, and the seasonal and diurnal variations in carbon fluxes to be calculated by the model. The advantage of simulating the annual mean and seasonal variations separately is that we can analyze the contribution of nonlinear interactions between the time-varying component of the biotic fluxes and the atmospheric transport (Denning et al., 1995 and Part 2). Our approach is somewhat analogous to the use of "flux corrections" in coupled ocean-atmosphere models (Manabe et al., 1990). We acknowledge that the initial value problem of the soil carbon pools is intractable at this time, and therefore focus on the boundary value problem of seasonal and diurnal forcing and the atmospheric response. This approach precludes robust interpretation of our results for the annual net carbon flux (balanced everywhere), except in the context of the atmospheric inversion problem, which we will analyze in a later paper.

Our methodology is in contrast to that of Bonan (1995), who parameterized assimilation and respiration independently of one another. His results for the 5-year mean included a net annual sink of about 5 Gt C yr^{-1} (calculated from Table 6 of Bonan, 1995), with very strong regional sources

and sinks of CO_2 at the land surface. For example, he calculated that semiarid and arid lands were a net source of more than 5 Gt C yr^{-1}, mostly in the northern subtropical zone, with tropical and boreal forests and tundra acting as a combined net sink of more than 8 Gt C yr^{-1}. Such strong net annual sources and sinks would impose a meridional structure on the CO_2 concentration of the atmosphere of similar magnitude to that imposed by fossil fuel emissions (about 6 Gt C yr^{-1}, Schimel et al., 1995), which is inconsistent with the observational record. More recent calculations with a revised model give a much smaller annual net sink of about 1.3 Gt C yr^{-1}, distributed among boreal and tropical ecosystems (G. Bonan, personal communication). Such a direct calculation of the carbon budget of the terrestrial biosphere is potentially very useful, but is sensitively dependent on the initial carbon pools and other parameters used to estimate the one-way fluxes, which in turn are derived from data collected at a small number of locations around the world. We believe both our approach and Bonan's to be valid, and consider them to be complementary.

2.4. Experimental integration

The model was integrated on a 4° × 5° (latitude × longitude) grid with 17 levels at a 6-min time step for 5 simulated years starting from an initial condition taken from a previous run. Diagnostic output was saved as monthly means throughout the run, and multiyear means for each month and the annual mean were computed from these monthly output data. Selected variables were sampled hourly and saved for several grid cells to be compared with observational data sets in section 4.

To separate the effects of the simulated climate of the GCM and the SiB2 parameterization on the simulated carbon fluxes, we performed a second experiment in which SiB2 was driven off-line using climatological data derived from observations. This simulation is referred to as the "SiBDRV" experiment. Sources for the climatological driver data sets used in this experiment are listed in Table 1. Six-hourly surface analyses obtained from the European Center for Medium-Range Weather Forecasting (ECMWF) were interpolated to hourly values on the coarser CSU GCM grid for most of the variables. Daily

Table 1. *Data sources used to generate the input used by the off-line SiB2 simulations*

Variable	Height	Frequency	Sources
zonal wind	10 m	6 hourly	ECMWF
meridional wind	10 m	6 hourly	ECMWF
temperature	2 m	6 hourly	ECMWF
dew point temperature	2 m	6 hourly	ECMWF
friction velocity	land surface	6 hourly	ECMWF
sensible heat flux	land surface	6 hourly	ECMWF
latent heat flux	land surface	6 hourly	ECMWF
surface net shortwave radiation	land surface	6 hourly	ECMWF
surface net longwave radiation	land surface	6 hourly	ECMWF
surface albedo (snow-free)	land surface	6 hourly	ECMWF
total cloud cover	N/A	6 hourly	ECMWF
Snow water equivalent	land surface	accumulated	ECMWF
vegetation cover	land surface	monthly	SiB2
total precipitation	land surface	daily	station observations
precipitation diurnal cycle	land surface	monthly	CSU GCM

total station precipitation records obtained at the National Center for Atmospheric Research (NCAR) were interpolated to the $4° \times 5°$ GCM grid and were prescribed hourly using the diurnal cycle of precipitation from the GCM. The hourly forcing data thus obtained were linearly interpolated to the 6-min time step of the GCM, and the model was integrated for 1 year, representing conditions for 1987.

3. Carbon metabolism at global and regional scales

3.1. Annual mean

Gross primary production (GPP) is given by the integrated photosynthetic assimilation rate (A) which is calculated as discussed in subsection 2.2. Net primary production (NPP) is given by

$$NPP = GPP - R_a , \qquad (11)$$

where R_a is the rate of carbon released by autotrophic respiration, which is the sum of the respiration rates in the canopy (R_c), stems (R_{stem}), and roots (R_{root}) of the plants. Canopy respiration is calculated as described in subsection 2.2. Respiration by stems and roots is not calculated by SiB2, but following Ryan (1991), we assume that on an annual basis,

$$R_a = 0.6 \, GPP , \qquad (12)$$

so that NPP = 0.4 GPP.

We further assume that stem respiration is negligible relative to the uncertainty in NPP. Annual root respiration is then estimated as a residual:

$$R_{root} = GPP - NPP - R_c , \qquad (13)$$

where R_C is the canopy respiration rate.

The mean global NPP simulated by SiB2 in the GCM was 44.8 Gt C yr^{-1} (Table 2, Fig. 1a), which is within the range of previous estimates. Melillo et al. (1993) reported that the mean of 13 such estimates in the literature was 53.1 Gt C yr^{-1}, with a range from 40.5 Gt C yr^{-1} to 78.0 Gt C yr^{-1}. Global NPP in the SiBDRV experiment was about 10% higher (49.9 Gt C yr^{-1}, Fig. 1b). The geographic distribution of annual NPP in both the GCM and SiBDRV experiments is similar to those presented by Melillo et al. (1993) and Potter et al. (1993), with the largest values in the tropical forests and broad areas of relative maxima in the temperate and boreal forests.

Regionally, the GCM estimates are significantly lower than both SiBDRV (Fig. 1c) and previous estimates in eastern North America, southeastern South America, and much of India. Bonan (1995) also reported reduced NPP over central North America, which he attributed to unrealistically warm summer temperatures. Annual NPP simulated by the GCM is considerably higher than simulated by SiBDRV in western North America, the Andes, central Asia, and in most desert regions. In nearly all of these cases, the differences between

Table 2. *Components of annual carbon metabolism by biome (Gt C yr^{-1})*

Biome	Area (%)	GPP	R_C	R_{root}	NPP GCM	NPP SiBDRV	NPP CASA
broadleaf evergreen trees	12.5	29.7	5.4	12.4	11.9	16.4	18.0
broadleaf deciduous tree	1.1	1.1	0.2	0.5	0.4	0.5	0.7
broadleaf and needleleaf trees	2.0	2.3	0.3	1.1	0.9	1.1	1.3
needleleaf evergreen trees	11.6	11.4	1.4	5.5	4.6	4.5	3.6
needleleaf-deciduous trees	5.5	4.0	0.4	2.0	1.6	1.8	1.0
broadleaf trees w/ groundcover	13.5	30.8	1.5	17.0	12.3	13.7	10.4
grasslands	7.4	6.4	0.3	3.5	2.5	1.9	1.9
broadleaf shrubs w/ groundcover	1.4	2.6	0.1	1.4	1.0	0.8	1.1
broadleaf shrubs with bare soil	6.4	4.7	0.7	2.1	1.9	0.5	1.2
tundra	4.2	1.0	0.1	0.5	0.4	0.4	0.5
desert	12.5	1.9	0.1	1.0	0.8	0.3	0.5
cultivation/C$_3$ grassland	21.9	16.1	2.3	7.4	6.4	7.9	7.8
total		111.9	12.7	54.5	44.8	49.9	48.0

GCM and SiBDRV NPP are due to unrealistic regional distribution of precipitation in the GCM (Fig. 1d). The GCM systematically overestimates orographic precipitation, leading to high annual NPP in regions of elevated terrain, and to underestimated precipitation (and therefore NPP) downstream of such regions. In addition, the precipitation associated with the Asian monsoon is under-represented in the GCM, resulting in lower simulated NPP in India and southeast Asia than simulated in the SiBDRV experiment. Regional undersimulation of precipitation causes soils to dry out, leading to extreme root zone water stress (Fig. 1e) in the areas noted above where NPP simulated by the GCM is well below that simulated by SiBDRV.
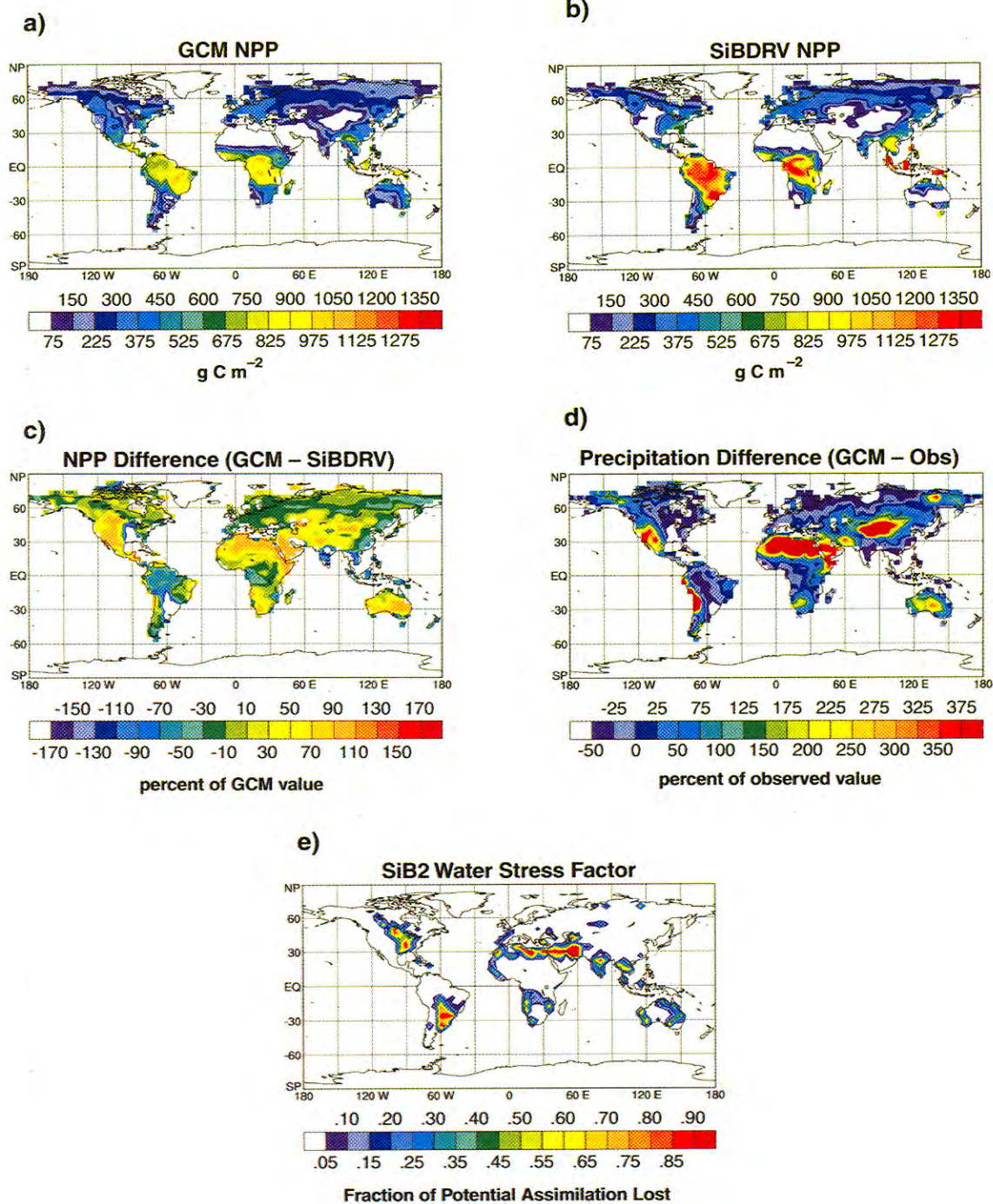
As simulated in the GCM, canopy and root respiration account for 11% and 49% of global GPP, respectively (Table 2). Fan et al. (1990) reported above ground respiration to be about 18% of GPP for a tropical rain forest site in Brazil which matches our estimate for that biome. For a broadleaf deciduous forest, Wofsy et al. (1993) reported that more than 80% of ecosystem respiration is from below ground sources (roots and soil heterotrophs); we estimate this fraction to be 82% for that biome.

The greatest differences in annual NPP between the GCM and SiBDRV simulations are in the tropical forests, where the SiBDRV estimate is 38% higher. In semiarid grasslands and shrublands, the GCM simulates higher NPP than SiBDRV, mostly due to the greater-than-observed precipitation in arid regions as noted above. Also presented in Table 2 are the NPP estimates of Potter et al. (1993) using the Carnegie-Ames-Stanford (CASA) biosphere model (forced with observed climate data). These estimates are qualitatively similar to both the GCM and SiBDRV simulations, but are higher in tropical forests and lower in the boreal evergreen forests.

In general, the agreement between the NPP calculation presented here and those of previous studies is encouraging, although of course it is quite possible the models are "converging" on a solution that does not reflect the real world. In

Fig. 1. (a) Annual net primary production (g C m^{-2} yr^{-1}) simulated by SiB2 in the GCM (4 year mean). (b) Annual net primary production (g C m^{-2} yr^{-1}) simulated in the SiBDRV experiment, in which SiB2 was driven off-line using climatological data derived from observations. (c) The difference between the GCM and SiBDRV-simulated NPP, as a percentage of the GCM value. (d) The difference between the annual total precipitation simulated by the GCM and the climatology of Legates and Willmott (1990), as a % of the climatological value. (e) Annual mean root zone water stress factor diagnostic (4 year mean) calculated by SiB2 in the GCM simulation. Values indicate the fractional reduction of canopy net assimilation from the unstressed value.

a)

GCM NPP

150 300 450 600 750 900 1050 1200 1350

75   225 375 525 675 825 975 1125 1275

g C m^{-2}

b)

SiBDRV NPP

150 300 450 600 750 900 1050 1200 1350

75   225 375 525 675 825 975 1125 1275

g C m^{-2}

c)

NPP Difference (GCM – SiBDRV)

-150 -110 -70 -30   10   50   90 130 170

-170 -130 -90 -50 -10   30   70 110 150

percent of GCM value

d)

Precipitation Difference (GCM – Obs)

-25   25   75 125 175 225 275 325 375

-50   0   50 100 150 200 250 300 350

percent of observed value

e)

SiB2 Water Stress Factor

.10 .20 .30 .40 .50 .60 .70 .80 .90

.05 .15 .25 .35 .45 .55 .65 .75 .85

Fraction of Potential Assimilation Lost

some regions it is clear that the GCM simulation is producing much less biological activity than previous results have predicted, especially in those areas where the GCM-simulated precipitation is well below the observed annual values. This is a consequence of our approach of simultaneously simulating both the climate and the ecosystem metabolism, and is not surprising. When models of two complex systems are coupled, the results can be unrealistic even if the component models are each fairly well-behaved, as for example in coupled ocean-atmosphere simulations (Manabe et al., 1990). One advantage of this approach is the ability to integrate forward in an internally consistent manner and to investigate mechanisms of climate and carbon cycle change. Another is the ability to quantify the effect of covariance between the biotic surface fluxes and the transport which have a significant influence on the spatial structure of atmospheric CO_2 concentrations.

3.2. Seasonal cycle

The seasonal cycle of soil respiration (by both roots and heterotrophic microbes) is obtained from the annual mean estimates presented in the previous section by applying the seasonal cycle of the nondimensional respiration rate r, as defined in subsection 2.2:

$$R_{root}(x,t) = r(x,t)\langle R_{root}\rangle, \qquad (14)$$

where $\langle R_{root}\rangle$ is the annual total root respiration. Monthly mean NPP is then calculated as

$$NPP(x,t) = GPP(x,t) - R_C(x,t) - R_{root}(x,t). \qquad (15)$$

Note that this formulation allows negative NPP in cases where maintenance respiration by vegetation exceeds photosynthesis.

Monthly mean NPP as calculated in both the GCM and SiBDRV simulations is presented for January and July in Fig. 2a–d. Both experiments show very strong seasonality of NPP in the northern temperate and boreal regions, with slightly negative NPP in January followed by strongly positive NPP in July. In the tropics, changes in NPP are related to seasonal changes in precipitation rather than temperature. NPP is more seasonal in the tropics as simulated by SiBDRV than by the GCM, with approximately the same geographic distribution of NPP in the two extreme

seasons, but much higher amplitude in the SiBDRV experiment.

The stronger seasonal NPP in the tropics in the SiBDRV simulation is particularly evident in the growing season net flux (GSNF, Fig. 2e–f), defined here as the sum of net uptake of carbon at the land surface for months in which photosynthesis exceeded respiration (Fung et al., 1987, hereafter referred to as F87). This is a simple measure of the effect of the seasonal terrestrial biota on the amplitude of seasonal variations in atmospheric CO_2. Between 20°N and 20°S, the GSNF simulated by SiBDRV is nearly twice that simulated by the GCM. Seasonal carbon uptake is also stronger in the northern midlatitudes in the SiBDRV experiment than in the GCM experiment, with a zonal mean of 190 g C m^{-2} at 60°N in SiBDRV versus 145 g C m^{-2} in the GCM. Both experiments have stronger GSNF than was simulated by Potter et al. (1993). Their simulations showed only very small areas in the tropics with GSNF greater than 250 g C m^{-2}, and most of the boreal forest with GSNF between 50 and 150 g C m^{-2}.

The complete seasonal cycle of simulated zonal total carbon flux to the atmosphere from the land surface is compared to the earlier estimates of F87 in Fig. 3. Regionally, the strongest seasonal forcing for atmospheric CO_2 (highest GSNF) is in the tropics, but the zonally integrated forcing is much stronger in the middle northern latitudes, reflecting the much greater land area there. As noted above, the tropical fluxes are much more seasonal in the SiBDRV experiment than in the GCM experiment, with the F87 fluxes closer to the GCM than to SiBDRV. In all 3 panels, the drawdown of atmospheric CO_2 during the northern growing season is strongest at about 60°N, but the timing of this feature is nearly a month earlier as simulated by the GCM than the F87 estimates. The time of maximum drawdown in the SiBDRV simulation is intermediate. A long-standing discrepancy between the observed seasonal cycle at high northern latitudes and many simulations with tracer transport models driven by prescribed fluxes has been the tendency for the simulated concentration to rise too high and begin to decline too late in the boreal spring (F87, Tans et al., 1990; Denning, 1994). The springtime efflux is weaker and the timing of the spring drawdown is earlier as simu-
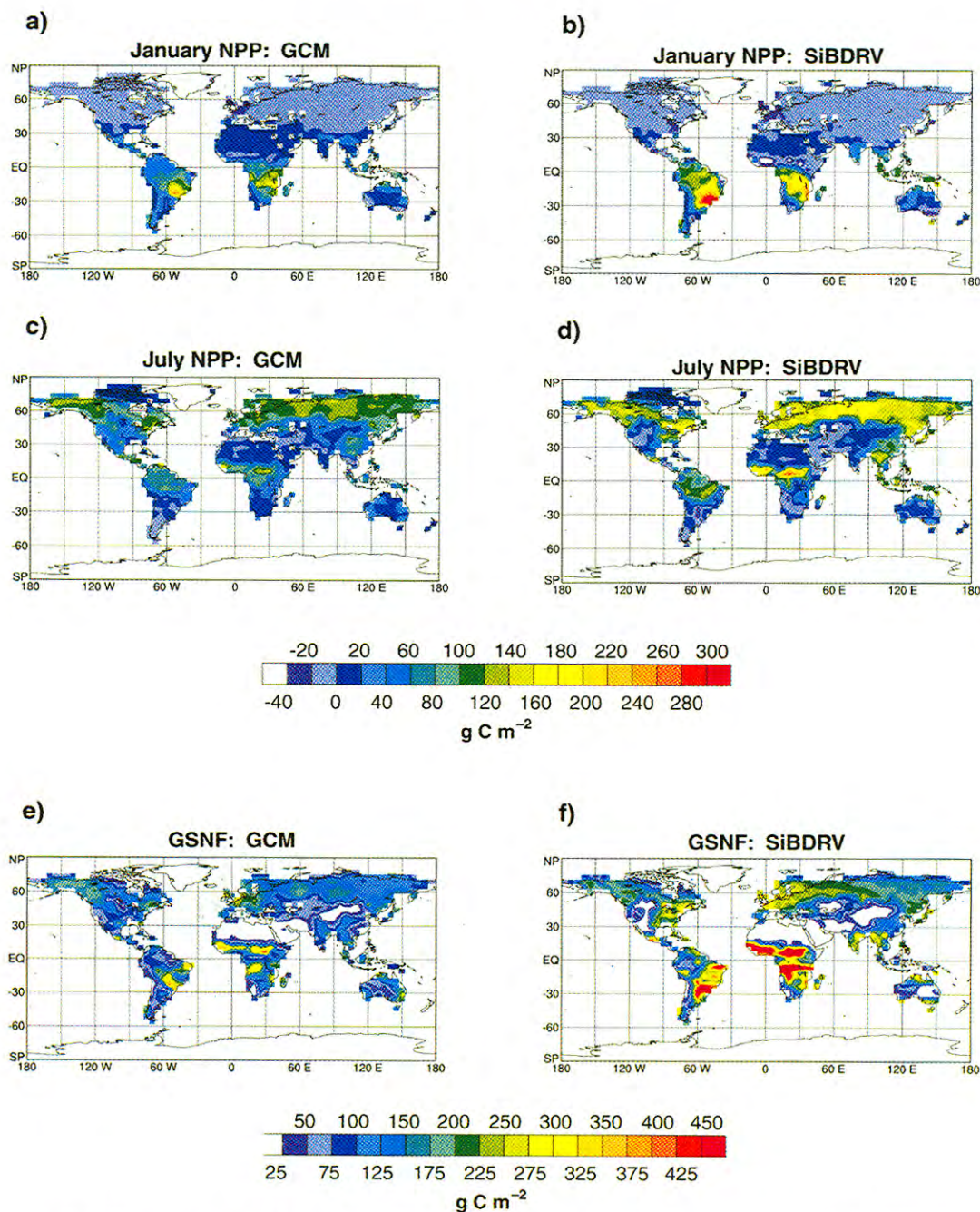
Fig. 2. (a) Monthly net primary production (g C m^{-2} month^{-1}) as simulated by SiB2 in the GCM for January (4 year mean). (b) Monthly net primary production (g C m^{-2} month^{-1}) as simulated by SiBDRV for January. (c) As in Fig. 2a, but for July. (d) As in Fig. 2b, but for July. (e) Growing season net carbon flux (defined in the text) as simulated by SiB2 in the GCM. (f) Growing season net carbon flux as simulated by SiBDRV. *Note.* The upper color bar refers to panels (a)–(d) and the lower color bar refers to panels (e) and (f).
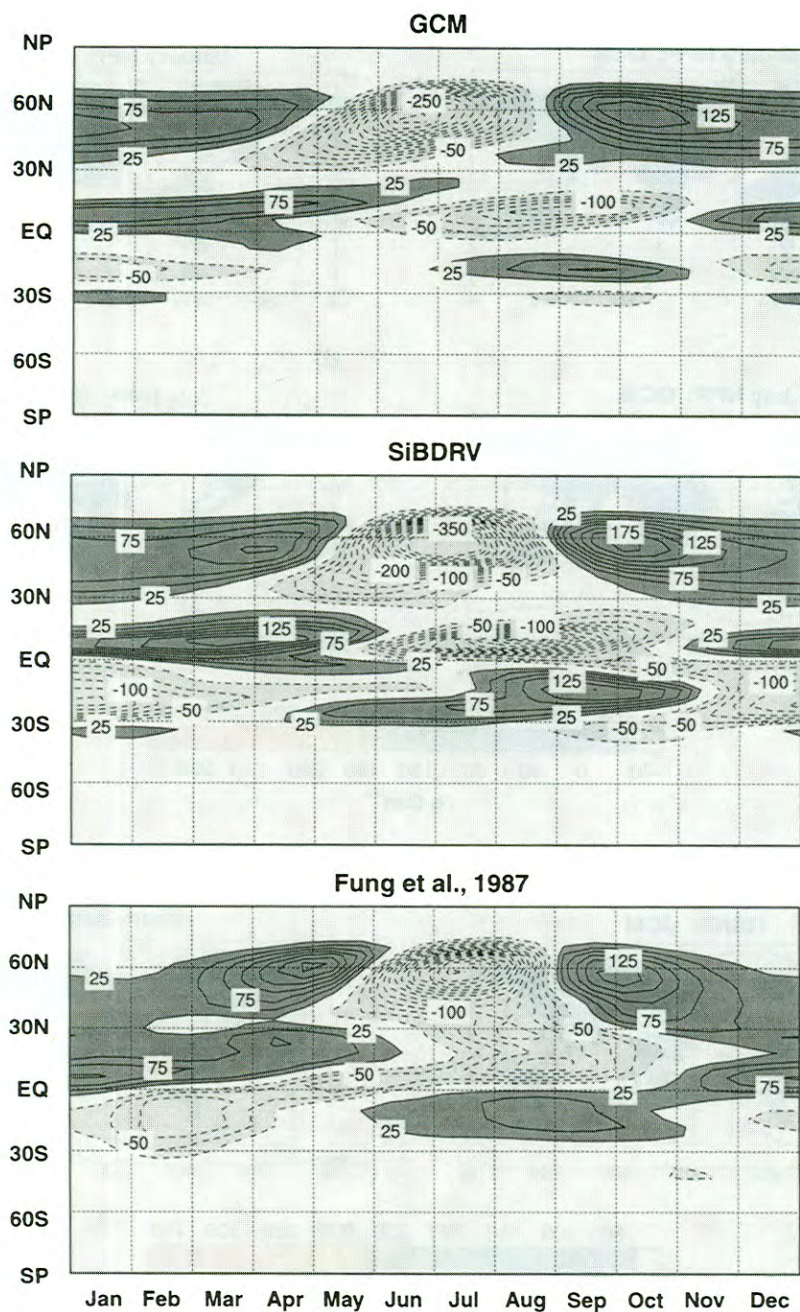
Fig. 3. Zonal total net flux of carbon (10^9 kg C month^{-1} per 4° latitude strip) from the land surface to the atmosphere by latitude and month of the year (a) as simulated by SiB2 in the GCM; (b) as simulated by SiBDRV; and (c) as calculated from the published estimates of Fung et al. (1987). The contour interval in all three panels is 25×10^9 kg C month^{-1} per 4° latitude strip, with dark hatching for values above 50 and light hatching for values below -50. For clarity, the zero contour has been omitted.

lated by SiB2, which is probably more realistic than the F87 scenario.

Net carbon release due to respiration in the boreal and northern temperate zones is a maximum in the fall, and then decreases monotonically until spring as simulated in the GCM, but in SiBDRV a secondary peak is simulated in spring. The simulated accumulation and melting of the snowpack tend to be later in both SiBDRV and the GCM than observed (Fig. 4), leading to simulated soil temperatures which are systematically warmer than observed in autumn and colder than observed in spring. This effect is stronger in the GCM than in SiBDRV because of feedbacks between the surface energy budget and the atmospheric thermal structure which are not present in SiBDRV, resulting in weaker springtime respiration in the GCM. Net respiration from boreal ecosystems is confined almost entirely to the spring and fall in the F87 estimates, but is more gradual and occurs throughout the winter as simulated by SiB2. This is partly due to the fact that F87 used climatological air temperature to estimate the respiration rate, whereas SiB2 uses the soil temperature (6), which has less seasonal amplitude due to its heat capacity.

The simulated carbon metabolism using SiB2 in the GCM is in general agreement with previous global estimates, both in terms of a geographic distribution in the annual mean NPP and in terms of the seasonal cycle of the carbon fluxes to the atmosphere. Comparison of the GCM results to those of the SiBDRV experiment indicates that most of the differences between our results and those of previous studies are related to inaccurate simulation of precipitation by the GCM. This suggests that the mismatch between the climate simulated by the GCM and the prescribed realistic vegetation distribution in SiB2 may result in reduced seasonal amplitude of the surface carbon flux in the model relative to the real world. Denning et al. (1995) showed that covariance of the seasonal fluxes and seasonal changes in atmospheric circulation in the middle to high northern latitudes can have a strong influence on the meridional gradient of CO_2 in the annual mean. If in fact the GCM underestimates the seasonal amplitude of the carbon flux in this region, then it may underestimate the annual mean gradient as well. This possibility is explored further in Part 2.

4. Comparison to observations of carbon metabolism

Most observational data regarding exchanges of CO_2 between the atmosphere and the terrestrial biota are collected for short periods of time at spatial scales that are too small to allow meaningful comparison with a GCM simulation (commonly at the scale of a single leaf or plant). Flux data from eddy correlation studies provide the most useful tool for model validation in this context because they represent CO_2 exchange at the canopy level. Unfortunately, long-term eddy correlation studies of canopy carbon exchange have been performed at only a few widely separated locations. In this section we evaluate the realism of the seasonal and diurnal cycles in the model by analyzing the simulated carbon fluxes at specific grid points in the model which represent the locations of field studies in several different biomes (Fig. 5).

The simulated fluxes in the temperate forest are compared with eddy correlation data collected at Harvard Forest (Wofsy et al., 1993; Goulden et al., 1996). The GCM grid cell representing Harvard Forest is classified as cropland by SiB2, so the results shown here are for the grid point immediately northeast of the one containing the coordinates of the field site. Simulated fluxes at a tropical forest grid cell representing Manaus, Brazil are compared to observations made as part of the Amazon Boundary Layer Experiment (ABLE) (Wofsy et al., 1988; Fan et al., 1990). The simulated temperate grassland fluxes are compared to data collected during the First ISLSCP Field Experiment (FIFE, Sellers et al., 1992b) (data provided by S. Verma, personal communication).

4.1. Seasonal cycle

At the Harvard Forest and ABLE sites, the net ecosystem exchange of CO_2 is computed from the eddy correlation measurements according to

$$\mathrm{NEE} = \overline{w'C'}(z_{\mathrm{m}}) + \frac{\mathrm{d}}{\mathrm{d}t} \int_0^{z_{\mathrm{m}}} C(z)\mathrm{d}z, \qquad (16)$$

where w is the vertical wind speed, C is the mixing ratio of CO_2, z is height above the ground, and z_{m} is the height at which the eddy fluxes are calculated. The 1st term on the right-hand-side of
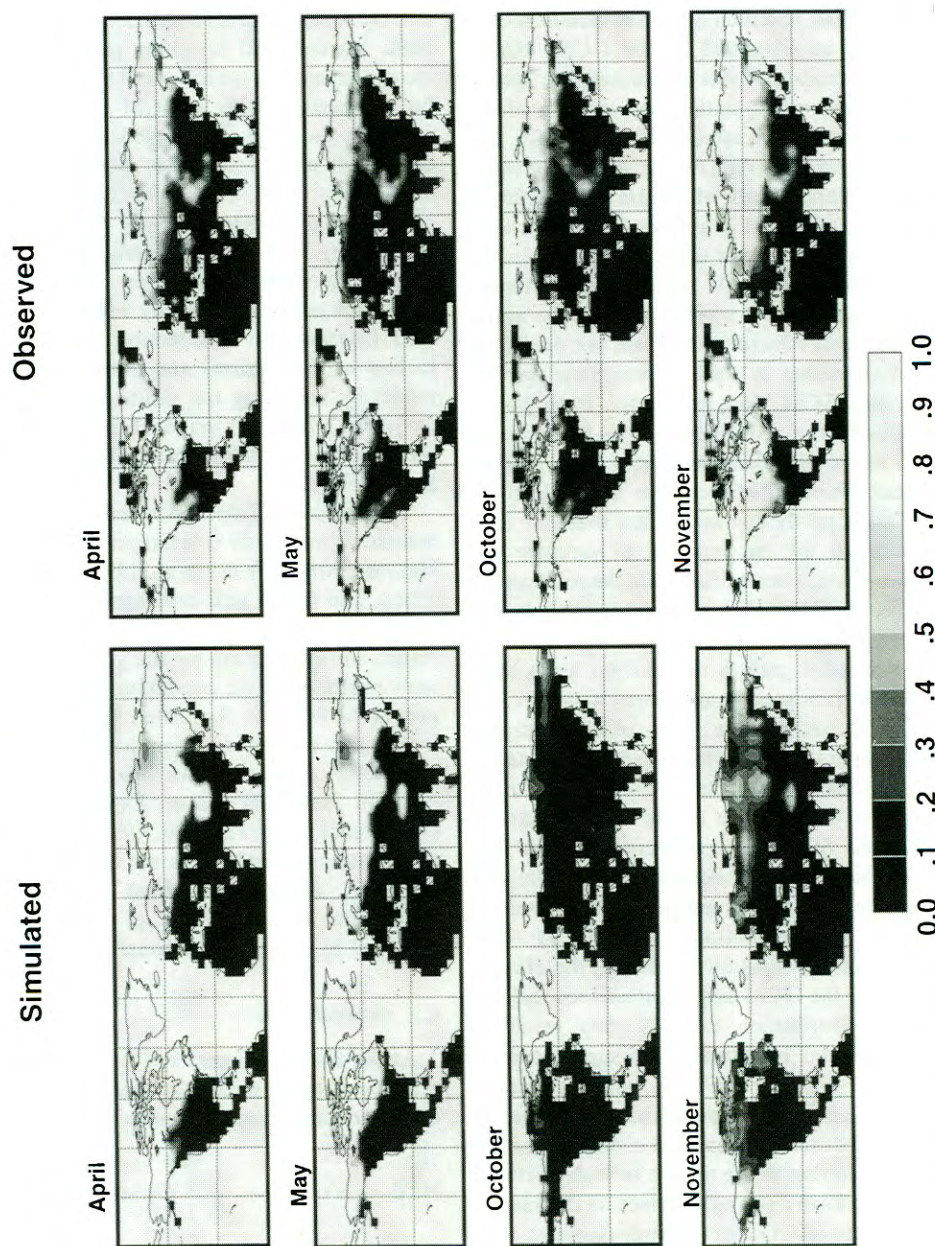
Snow Cover Fraction on 4x5 Degree Grid

Fig. 4. Comparison of areal coverage of the land surface by snow as simulated by SiB2 (left panels), and as calculated from visible satellite imagery (Dewey and Heim, 1982) for 1982–1991. Observational data are monthly means, and have been averaged onto the 4° × 5° grid of the CSU GCM.
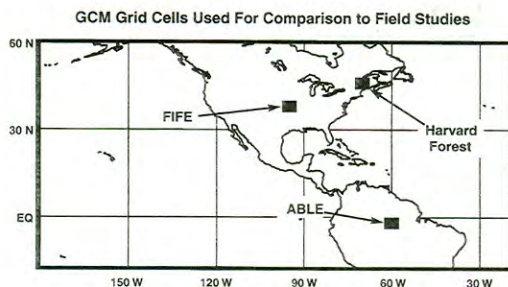
Fig. 5. Locations of 3 GCM grid cells used to compare the simulated carbon fluxes to observational data.

(16) represents the upward flux of CO_2 through the instrument level, and the 2nd term represents the change in storage of CO_2 below that level.

The simulated seasonal cycle of monthly mean GPP, ecosystem respiration, and NEE at each of the three grid locations in Fig. 5 is presented in Fig. 6, along with the available observations. At the temperate forest (Fig. 6a and 6b) grid point, the observational data are plotted as monthly means. In the tropical forest (Fig. 6c), observed mean values are only available for short periods in July of 1985 (Wofsy et al., 1988), and late April to early May of 1987 (Fan et al., 1990). At the FIFE site, CO_2 flux measurements sampled the diurnal cycle adequately for daily means to be calculated only for four periods of a few days each. These data were averaged over the diurnal cycle for each of these periods and are plotted in Fig. 6d.

The amplitude of the simulated seasonal cycle of each flux component varies widely among the three sites, with the temperate forest showing the strongest seasonality and the tropical forest showing almost none. The net CO_2 flux to the atmosphere is a smaller residual between the large opposing fluxes due to assimilation and respiration, and depends sensitively on phase differences between these components. The monthly mean NEE is near zero all year in the tropical forest although both photosynthesis and respiration are very strong, whereas the slight lag in the phase of seasonal carbon assimilation relative to respiration in the temperate forest results in large and highly seasonal NEE values.

The phase of the seasonal cycle is well simulated by the GCM at the temperate forest site (Fig. 6a), but the amplitude of the simulated GPP is weaker

than observed by Wofsy et al. (1993). Results for this grid point shown in Fig. 6b are from an experiment conducted while this paper was in review, but for which atmospheric transport and concentration of CO_2 was not simulated. The biosphere model is unchanged in the new simulation, but the simulated climate over much of the land surface of the world is noticeably more realistic. The annual grid cell mean precipitation in the new simulation is 1038 mm, vs. 821 mm in the original experiment, and 1135 mm in the gridded climatology of Legates and Willmott (1990). Wofsy et al. (1993) calculate that this site was a net sink for atmospheric CO_2 of 370 g C m^{-2} yr^{-1}, whereas we have constrained SiB2 to produce exact carbon balance in the annual mean at each grid point (see Section 2.2). In Fig. 6b, we have adjusted the respiration rates to produce the observed annual uptake. The simulated GPP and NEE are now in much closer agreement with the observations, suggesting that the earlier underestimates were a result of chronic drought stress due to a dry simulated climate rather than systematic errors in SiB2.

At the other 2 sites, the observational data do not permit separate evaluation of the flux components, nor do they span the year sufficiently to provide much of a constraint on the simulated seasonal cycle of NEE. At each site the magnitude of the observed net flux is fairly well captured by the GCM during the growing season, showing that the coupled model provides plausible estimates of the magnitude and timing of the seasonal exchange of CO_2 between the atmosphere and the tropical and temperate forest and the temperate grassland. In each case the model tends to err on the side of underestimating the amplitude of the seasonal cycle of the fluxes. This suggests that the simulated effect of covariance between seasonal fluxes and seasonal transport will be a lower bound rather than an overestimate (Denning et al., 1995).

4.2. Diurnal cycle

The diurnal cycle of net assimilation, soil respiration (sum of R_{root} and R_{micr}), and net flux are presented for the three field locations in Fig. 7, along with diurnal variations of the net flux derived from the observational data. The simulated fluxes are diurnal composites over a month.
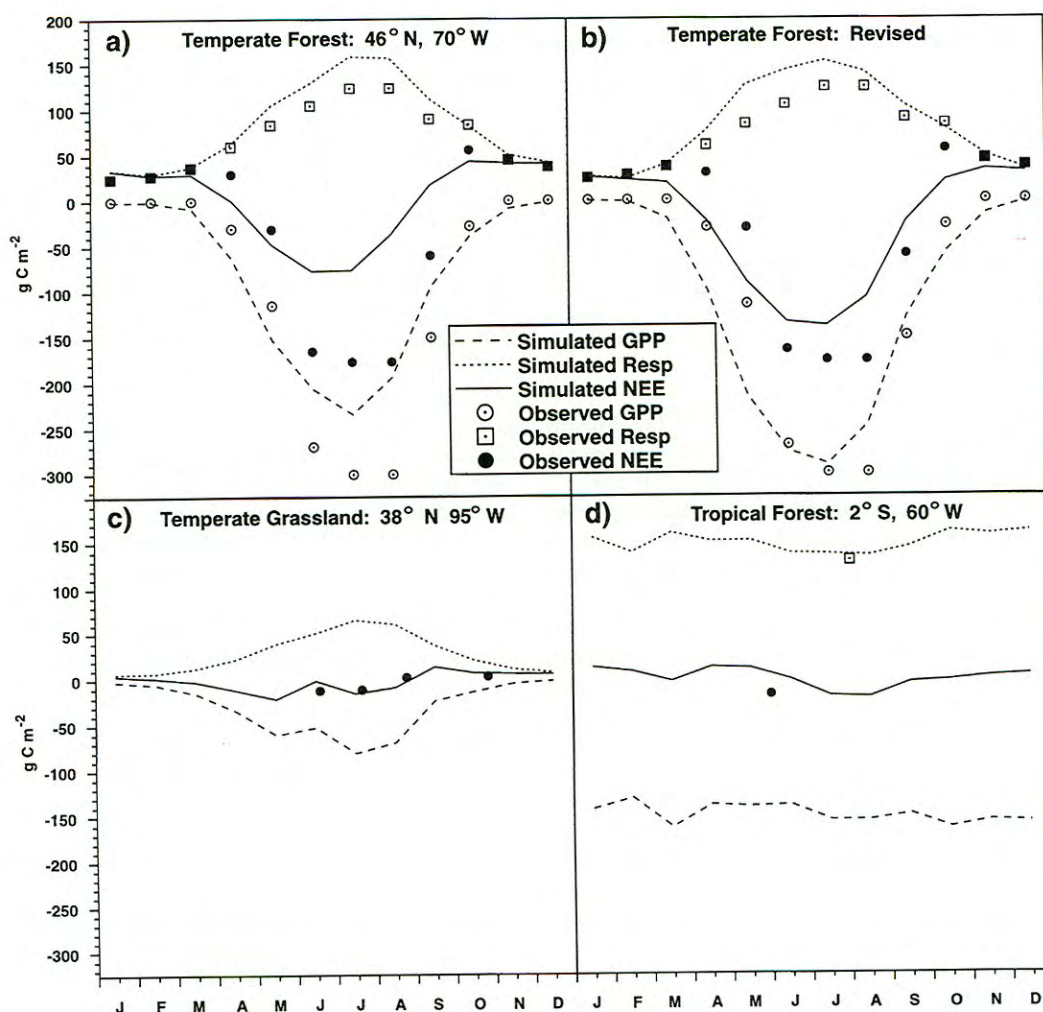
Fig. 6. Simulated seasonal cycles of gross primary production (GPP), ecosystem respiration, and net carbon flux (all in g C m^{-2} month^{-1}) at the 3 grid cells indicated in Fig. 5, for the final year of the GCM simulation. Where available, fluxes derived from observations are indicated as well. Panel (b) shows results for an experiment performed while this paper was in review, which did not include the calculation of CO_2 transport in the atmosphere.

The Harvard Forest data are means for each hour of the day over two 10-day periods in late June and late July of 1991. The FIFE data were collected in late July and early August of 1987. The ABLE data are means for each hour between April 22 and May 8, 1987. At all three sites, diurnal variations in the soil respiration fluxes are weak, with nearly all the variation in the net flux being driven by the diurnal cycle of photosynthesis. The simulated net flux at all 3 sites is a maximum in late morning, with a pronounced

mid-day depression evident at the temperate forest and temperate grassland sites.

In the temperate forest, the phase of the seasonal cycle is well simulated (Fig. 7a), but the observed uptake at midday is nearly twice as intense in the observations than the GCM, and the observations show no depression in photosynthesis as is simulated. This is consistent with the much larger monthly mean GPP in the observations as discussed above. In the tropical forest, the simulated phase of the fluxes again matches the observations

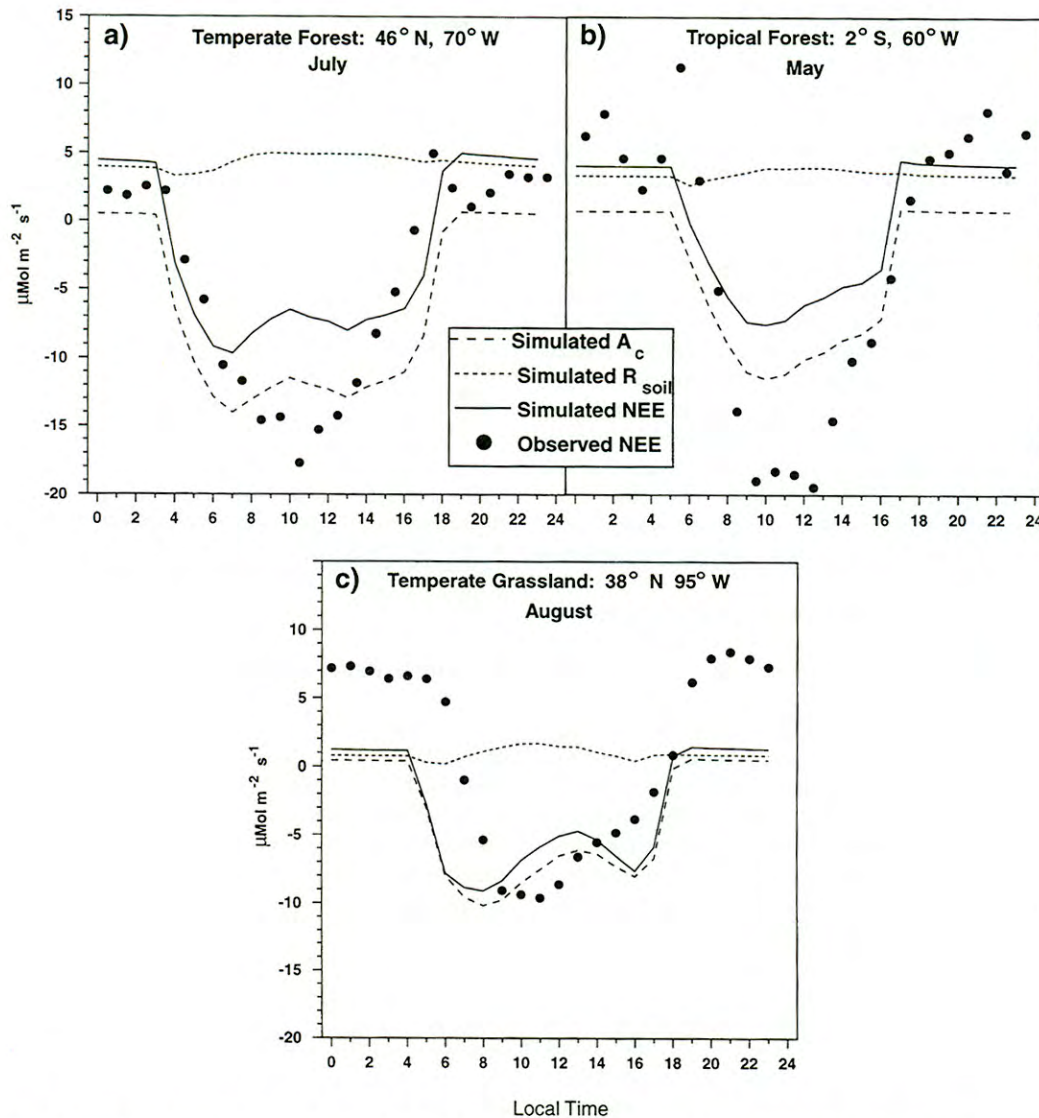## Simulated and Observed Diurnal Cycles

Fig. 7. Simulated monthly mean diurnal cycle of net canopy carbon assimilation (A_c), soil respiration (R_{soil}), and net ecosystem exchange (NEE), all in µMol m^{-2} s^{-1}, at the 3 locations indicated in Fig. 5, for various months in the final year of the GCM simulation. The net flux derived from eddy correlation measurements is indicated for comparison.

well, but the observed NEE at mid-day is about twice as strong as simulated by the GCM (Fig. 7b). Respiration efflux of CO_2 at night is also somewhat higher in the observations, but the simulation

may produce the more realistic estimate in this case. Fan et al. (1990) note that there is a significant bias toward sunny conditions in the data, such that their estimate of total net CO_2 uptake is

nearly 75% less than computed directly by averaging the available flux data. Applying such a correction to the diurnal composite in Fig. 7b would bring the observational results very close to the simulated NEE.

At the temperate grassland site in August, the phase of the net flux is about right, and the midday uptake is about the same as observed, but the nocturnal respiration flux is much greater in the observations than in the GCM (Fig. 7c). As discussed in subsection 3.1, simulated annual NPP in this region is much lower than previous estimates (or the SiBDRV simulation) due to inadequate simulated precipitation. Because the respiration fluxes in SiB2 are scaled by the annual total carbon assimilation, the unreasonably low annual GPP leads to significant underestimation of respiration fluxes as well. Part of the discrepancy between the simulation and the observations may be due to differences in sampling frequency. The GCM results are true diurnal composites over every hour in the month, whereas the observations were taken over a shorter period and contain missing data.

The August composite diurnal cycle simulated by SiBDRV for the FIFE site (Fig. 8) is still considerably weaker than observed, although stronger than as simulated in the GCM. Undersimulation of the respiration flux accounts for most of the discrepancy, as shown by the good agreement during daylight hours and poor agreement at night. Although the SiBDRV simulation is driven by data derived from observations, it is prescribed at the grid scale ($4° \times 5°$), so that local conditions may not be well represented. In addition, soil hydrological and thermal variables are calculated prognostically in SiBDRV, so soil moisture or temperature may be unrealistic even if the atmospheric forcing is accurate. When the fluxes are simulated by SiB2 (Berry et al., 1996) using all available site meteorological and hydrological data (as opposed to the SiBDRV experiment which uses gridded data products), the agreement is excellent, both for individual days (Fig. 9a) and over the whole season (Fig. 9b). This simulation benefits from the use of observed soil moisture profiles, suggesting that in addition to the above-noted undersimulation of precipitation in the GCM in this region, the parameterization of soil hydrology in SiB2 may be failing to maintain realistic amounts of moisture.
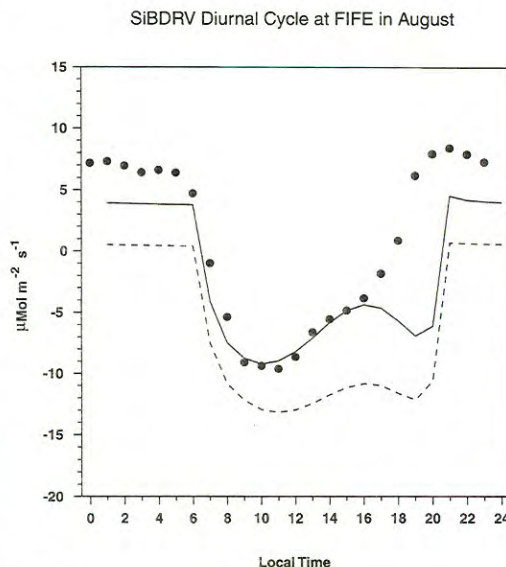

Fig. 8. Simulated monthly mean diurnal cycle of net canopy carbon assimilation (A_c), soil respiration (R_{soil}), and net ecosystem exchange (NEE) ($\mu Mol\ m^{-2}\ s^{-1}$), as simulated by SiBDRV at the FIFE grid cell for August of 1987.

5. Summary and conclusions

This study represents the first effort to predict the seasonal and diurnal exchange of carbon between the atmosphere and terrestrial biosphere at the global scale using a coupled biosphere-climate model. The simulated carbon balance is intentionally closed at each grid point at the annual time scale, avoiding the large transient fluxes that have characterized previous studies. Given the highly interactive nature of the coupled model, it is encouraging that the predicted exchange of CO_2 produced global estimates of carbon fluxes that are within the range reported by previous studies, with a similar geographic distribution of annual NPP and GSNF. Significant regional differences occur where precipitation simulated by the GCM is less than observed, and nearly always lead to lower calculated NPP in the GCM than in the SiBDRV experiment where SiB2 was forced by climate data derived from observations. The largest differences in NPP between the GCM and SiBDRV experiments are found in the tropical forests, but the largest fractional differences are in the central

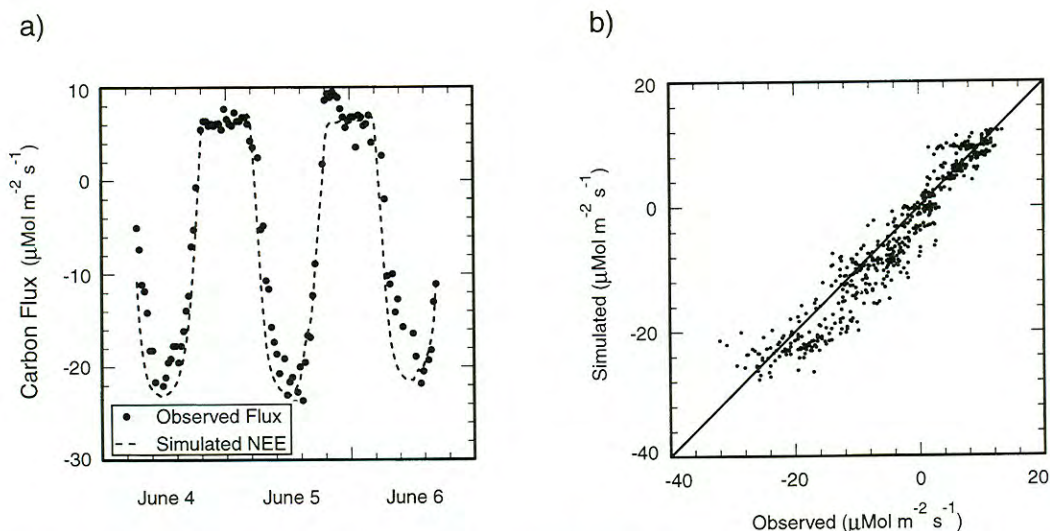## FIFE Simulations Forced by Observations

a)

b)

Fig. 9. Simulated NEE and observed site carbon flux at the FIFE site, station 16, in the summer of 1987. SiB2 was driven by observed site meteorological and hydrological data. Data provided by S. Verma, personal communication. (a) Time series for three days in early June. (b) Scatter plot of simulated NEE *vs.* observed flux over 142 days of the growing season.

United States, Argentina, and southeast Asia, where the simulated climate is particularly dry relative to the observations.

The seasonal cycle of surface exchange of CO_2 is strongest in the northern temperate and boreal zones, with a geographic distribution that is very similar to earlier estimates of the fluxes by F87. The seasonal cycle is weaker in the tropics as simulated by the GCM than as simulated by SiBDRV, but somewhat stronger than in the F87 estimates. Because the GCM uses soil temperature rather than air temperature to estimate the seasonal distribution of respiration, small amounts of CO_2 are released from temperate and boreal soils throughout the winter, unlike the F87 estimates which show a larger efflux of CO_2 from this zone in spring.

The simulated seasonal and diurnal cycles of monthly mean carbon fluxes agree fairly well with the very limited observations available, at least in terms of the net flux. The GCM has a tendency to underestimate the intensity of mid-day carbon uptake relative to the observations at several locations. This problem is the result of root zone

water stress due to chronic under-simulation of precipitation at many locations. GCM results obtained while this paper was in review show significant improvement in the simulated precipitation over many continental areas, so the simulated carbon fluxes are expected to increase in future experiments.

In nearly all cases where discrepancies between the simulated and observed carbon fluxes can be identified, the simulated fluxes are too weak during periods of intense vertical mixing in the atmosphere due to PBL turbulence and cumulus convection (i.e., mid-day at mid-summer). This is expected to result in systematic underestimation of the strength of the meridional gradient of atmospheric CO_2 imposed by correlations between the simulated fluxes and transport (Denning et al., 1995).

6. Acknowledgments

We are grateful to Prof. Shashi Verma of the University of Nebraska, who graciously provided

REFERENCES

Arakawa, A. and Schubert, W. H. 1974. Interaction of a cumulus cloud ensemble with the large-scale environment, Part I. *J. Atmos. Sci.* **31**, 674–701.

Arakawa, A. and Lamb, V. R. 1977. Computational design of the basic dynamical processes of the UCLA general circulation model. *Methods in Computational Physics* **17**, 173–265.

Arakawa, A. and Lamb, V. R. 1981. A potential enstrophy and energy conserving scheme for the shallow water equations. *Mon. Wea. Rev.* **109**, 18–36.

Ball, J. T. 1988. *An analysis of stomatal conductance.* PhD Thesis, Stanford University, Stanford, Calif.

Berry, J. A., Sellers, P. J., Randall, D. A., Collatz, G. J., Colello, G. D., Denning, A. S., Fu, W. and Grivet, C. 1996. SiB2, a model for simulation of biological processes within a climate model. In: *Scaling up* (eds. P. van Gardingen, G. Moody and P. Curran), Society for Experimental Biology, Cambridge University Press, in press.

Bonan, G. B. 1995. Land-atmosphere CO_2 exchange simulated by a land surface process model coupled to an atmospheric general circulation model. *J. Geophys. Res.* **100**, 2817–2831.

Collatz, G. J., Ball, J. T., Grivet, C. and Berry, J. A. 1991. Physiological and environmental regulation of stomatal conductance, photosynthesis, and transpiration: a model that includes a laminar boundary layer. *Agric. and Forest Meteorol.* **54**, 107–136.

Collatz, G. J., Ribas-Carbo, M. and Berry, J. A. 1992. Coupled photosynthesis-stomatal conductance model for leaves of C_4 plants. *Aust. J. Plant Physiol.* **19**, 519–538.

Dai, A. and Fung, I. Y. 1993. Can climate variability contribute to the "missing" CO_2 sink? *Global Biogeochem. Cycles* **7**, 599–610.

Denning, A. S. 1994. Investigations of the transport, sources, and sinks of atmospheric CO_2 using a general circulation model. *Atmospheric Science Paper* **564**, Colorado State University.

Denning, A. S., Fung, I. Y. and Randall, D. A. 1995. Latitudinal gradient of atmospheric CO_2 due to seasonal exchange with land biota. *Nature* **376**, 240–243.

Denning, A. S., Randall, D. A., Collatz, G. J., and Sellers, P. J. Simulations of terrestrial carbon metabolism and atmospheric CO_2 in a general circulation model. Part 2: Spatial and temporal variations of atmospheric CO_2. *Tellus* **48B**, this issue.

Dewey, K. F. and Heim, R. 1981. *Satellite observations of variations in Northern Hemisphere seasonal snow cover.* NOAA technical report NESS 87. United States Department of Commerce, Washington, DC.

Dixon, R. K., Brown, S. and Houghton, R. A. 1994. Carbon pools and flux of global forest ecosystems. *Science* **263**, 185–190.

Enting, I. G. and Mansbridge, J. V. 1989. Seasonal sources and sinks of atmospheric CO_2. Direct inversion of filtered data. *Tellus* **39B**, 318–325.

Enting, I. G. and Mansbridge, J. V. 1991. Latitudinal distribution of sources and sinks of CO_2: Results of an inversion study. *Tellus* **43B**, 156–70.

Enting, I. G., Trudinger, C. M. and Francey, R. J., 1995. A synthesis inversion of the concentration and delta ^{13}C of atmospheric CO_2. *Tellus* **47B**, 35–52.

Fan, S.-M., Wofsy, S. C., Bakwin, P. S., Jacob, D. J. and Fitzjarrald, D. R. 1990. Atmosphere-biosphere exchange of CO_2 and O_3 in the central Amazon forest. *J. Geophys. Res.* **95**, 16851–16864.

Farquhar, G. D., Von Caemmerer, S. and Berry, J. A., 1980. A biochemical model of photosynthetic CO_2 assimilation in C_3 plants. *Planta* **149**, 78–90.

Foley, J. A. 1994. Net primary productivity in the terrestrial biosphere: The application of a global model. *J. Geophys. Res.* **99**, 20773–20783.

Fowler, L. A., Randall, D. A. and Rutledge, S. A. 1996. Liquid and ice cloud microphysics in the CSU General Circulation Model. Part I: Model description and simulated microphysical processes. *J. Clim.* **9**, 489–529.

Fowler, L. A. and Randall, D. A. 1996. Liquid and ice cloud microphysics in the CSU general circulation model. Part II: Impact on cloudiness, the Earth's radiation budget, and the general circulation of the atmosphere. *J. Clim.* **9**, 530–560.

Fowler, L. A. and Randall, D. A. 1996. Liquid and ice cloud microphysics in the CSU General Circulation Model. Part III: Sensitivity to modeling assumptions. *J. Clim.* **9**, 561–586.

Francey, R. J., Tans, P. P., Allison, C. E., Enting, I. G., White, J. W. C. and Trolier, M. 1995. Changes in oceanic and terrestrial carbon uptake since 1982. *Nature* **373**, 326–330.

Friedlingstein, P., Muller, J. F. and Brasseur, G. P. 1994. Sensitivity of the terrestrial biosphere to climate changes: Impact on the carbon cycle. *Environment. Pollut.* **83**, 143–46.

Friedlingstein, P., Fung, I., Holland, E., John, J., Brasseur, G. Erickson, D. and Schimel, D. 1995. On the contribution of CO_2 fertilization to the missing biospheric sink. *Global Biogeochem. Cycles* **9**, 541–556.

Fung, I., Prentice, K., Matthews, E., Lerner, J. and

Russell, G. 1983. Three-dimensional tracer model study of atmospheric CO_2: Response to seasonal exchanges with the terrestrial biosphere. *J. Geophys. Res.* **88**, 1281–1294.

Fung, I. Y., Tucker, C. J. and Prentice, K. C. 1987. Application of very high resolution radiometer vegetation index to study atmosphere-biosphere exchange of CO_2. *J. Geophys. Res.* **92**, 2999–3015.

Gifford, R. M. 1994. The global carbon cycle: a viewpoint on the missing sink. *Aust. J. Plant Physiol.* **21**, 1–5.

Goulden, M. L., Munger, J. W., Fan, S.-M., Daube, B. C. and Wofsy, S. C. 1996. Exchange of carbon dioxide by a deciduous forest: Response to interannual climate variability. *Science* **271**, 1576–578.

Hall, C. A. S., Ekdahl, C. A. and Wartenberg, D. E. 1975. A fifteen-year record of biotic metabolism in the northern hemisphere. *Nature* **255**, 136–38.

Harshvardhan, Davies, R., Randall, D. A. and Corsetti, T. G. 1987. A fast radiation parameterization for general circulation models. *J. Geophys. Res.* **92**, 1009–1016.

Heimann, M. and Keeling, C. D. 1989. A three-dimensional model of atmospheric CO_2 transport based on observed winds (2). Model description and simulated tracer experiments. In: *Aspects of climate variability in the Pacific and Western Americas, Geophysical Monograph* **55** (ed. D. H. Peterson). American Geophysical Union, Washington, D.C., pp. 237–275.

Heimann, M., Keeling, C. D. and Tucker, C. J. 1989. A three-dimensional model of atmospheric CO_2 transport based on observed winds (3). Seasonal cycle and synoptic time scale variations. In: *Aspects of climate variability in the Pacific and Western Americas, Geophysical Monograph* 55 (ed. D. H. Peterson). American Geophysical Union, Washington, DC, 277–303.

Keeling, C. D. 1958. The concentration and isotopic abundances of atmospheric carbon dioxide in rural areas. *Geochim. Cosmochim. Acta* **13**, 322–334.

Keeling, C. D., Bacastow, R. B., Carter, A. F., Piper, S. C., Whorf, T. P., Heimann, M., Mook, W. G. and Roeloffzen, H. 1989. A three-dimensional model of atmospheric CO_2 transport based on observed winds (1) Analysis of observational data. In: *Aspects of climate variability in the Pacific and Western Americas. Geophysical Monograph* 55 (ed. D. H. Peterson). American Geophysical Union, Washington, DC, 165–236.

Keeling, C. D., Piper, S. C. and Heimann, M. 1989. A three-dimensional model of atmospheric CO_2 transport based on observed winds. (4) Mean annual gradients and interannual variations. In: *Aspects of Climate Variability in the Pacific and Western Americas. Geophysical Monograph* 55 (ed. D. H. Peterson). American Geophysical Union, Washington, DC., 305–363.

Legates, D.R. and Willmott, C. J. 1990. Mean seasonal and spatial variability in gauge-corrected global precipitation. *Int. J. Climatology* **10**, 111–27.

Lieth, H. 1975. Modeling the primary productivity of the world. In: *Primary productivity of the biosphere* (ed.

H. Lieth and R. H. Whittaker) Springer-Verlag, New York, 237–263.

Lord, S. J., Chao, W. C. and Arakawa, A. 1982. Interaction of a cumulus cloud ensemble with the large-scale environment. Part IV. The discrete model. *J. Atmos. Sci.* **39**, 104–13.

Maisongrande, P., Ruimy, A. and Saugier, B. 1995. Monitoring seasonal and interannual variations of primary productivity, net primary productivity, and ecosystem productivity using a diagnostic model and remotely-sensed data. *Tellus* **47**, 178–190.

Manabe, S., Bryan, K. and Spelman, M. J. 1990. Transient response of a global ocean-atmosphere model to a doubling of atmospheric carbon dioxide. *J. Phys. Oceanogr.* **20**, 722–749.

Melillo, J. M., McGuire, A. D., Kicklighter, D. W., Moore B., Vorosmarty, C. J. and Schloss, A. L. 1993. Global climate change and terrestrial net primary productivity. *Nature* **363**, 234–240.

Potter, C. S., Randerson, J. T., Field, C. B., Matson, P. A., Vitousek, P. M., Mooney, H. A. and Klooster, S. A. 1993. Terrestrial ecosystem production: A process-oriented model based on global satellite and surface data. *Global Biogeochem. Cycles* **7**, 811–842.

Raich, J. W., Rastetter, E. B., Melillo, J. M., Kicklighter, D. W., Steudler, P. A. and Peterson, B. J. 1991. Potential net primary productivity of South America: Application of a global model. *Ecol. Applications* **1**, 399–429.

Randall, D. A., Harshvardhan, Dazlich, D. A. and Corsetti, T. G. 1989. Interactions among radiation, convection, and large-scale dynamics in a general circulation model. *J. Atmos. Sci.* **46**, 1943–970.

Randall, D. A., Harshvardhan, and Dazlich, D. A. 1991. Diurnal variability of the hydrologic cycle in a general circulation model. *J. Atmos. Sci.* **48**, 40–62.

Randall, D. A., Shao, Q. and Moeng, C.-H. 1992. A second-order bulk boundary-layer model. *J. Atmos. Sci.* **49**, 1903–923.

Randall, D. A. and Pan, D.-M. 1993. Implementation of the Arakawa-Schubert parameterization with a prognostic closure. In: *The representation of cumulus convection in numerical models* (eds. K. Emanuel and D. Raymond) American Meteorological Society, Boston, 137–144.

Randall, D. R., Sellers, P. J., Berry, J. A., Dazlich, D. A., Zhang, C., Collatz, J. A., Denning, A. S., Los, S. O., Field, C. B., Fung, I., Justice, C. O. and Tucker, C. J. 1996. A revised land-surface parameterization (SiB2) for GCMs. Part 3: The greening of the Colorado State University General Circulation Model. *J. Clim.* **9**, 738–763.

Ryan, M. G. 1991. Effects of climate change on plant respiration. *Ecol. Appl.* **1**, 157–67.

Schindler, D. W. and Bayley, S. E. 1993. The biosphere as an increasing sink for atmospheric carbon: Estimates from increased nitrogen deposition. *Global Biogeochem. Cycles*, **7**, 717–734.

Schimel, D., Enting, I. G., Heimann, M., Wigley, T. M.

L., Raynaud, D., Alves, D. and Siegenthaler, U. 1995. CO_2 and the carbon cycle. In: *Climate change 1994: radiative forcing of climate change and an evaluation of the IPCC IS92 emission scenarios* (eds. J. T. Houghton, L. G. Meira Filho, J. Bruce, H. Lee, B. A. Callander, E. Haites, N. Harris and K. Maskell). Cambridge University Press, Cambridge, 35–72.

Sellers, P. J., Mintz, Y., Sud, Y. C. and Dalcher, A. 1986. A simple biosphere model (SiB) for use within general circulation models. *J. Atmos. Sci.* **43**, 505–531.

Sellers, P. J., Shuttleworth, W. J., Dorman, J. L. Dalcher, A. and Robert, J. M. 1989. Calibrating the simple biosphere model for Amazonian tropical forest using field and remote sensing data. Part I: Average calibration with field data. *J. Appl. Meteor.* **28**, 727–759.

Sellers, P. J., Berry, J. A., Collatz, G. J., Field, C. B. and Hall, F. G. 1992. Canopy reflectance, photosynthesis, and transpiration (III). A reanalysis using enzyme kinetics—electron transfer models of leaf physiology. *Remote Sens. Environ.* **42**, 1–20.

Sellers, P. J., Hall, F. G., Asrar, G., Strebel, D. E. and Murphy, R. E. 1992. An overview of the 1st International Satellite Land Surface Climatology Project (ISLSCP) Field Experiment (FIFE). *J. Geophys. Res.* **97**, 18345–8371.

Sellers, P. J., Heiser, M. D. and Hall, F. G. 1992. Relations between surface conductance and spectral vegetation indices at intermediate (100 m^2 to 15 km^2) length scales. *J. Geophys. Res.* **97**, 19033–9059.

Sellers, P. J., Hall, F. G., Margolis, H., Kelly, B., Baldocchi, D., den Hartog, G., Chilar, J., Ryan, M. G., Goodison, B., Crill, P., Ranson, K. J., Lettenmaier, D. and Wickland, D. 1995. The Boreal Ecosystem-Atmosphere Study (BOREAS): An overview and early results from the 1994 year. *Bull. Amer. Meteorol. Soc.* **76**, 1549–577.

Sellers, P. J., Randall, D. A., Collatz, D. J., Berry, J. Field, C., Dazlich, D. A., Zhang, C. and Bounoua, L. 1996. A revised land-surface parameterization (SiB2) for atmospheric GCMs. Part 1: Model formulation. *J. Clim.* **9**, 676–705.

Sellers, P. J., Los, S. O., Tucker, C. J., Justice, C. O., Dazlich, D. A., Collatz, G. J. Randall, D. A. 1996. A revised land-surface parameterization (SiB2) for atmospheric GCMs. Part 2: The generation of global fields of terrestrial biophysical parameters from satellite data. *J. Clim.* **9**, 706–737.

Shine, K. P., Fouquart, Y., Ramaswamy, V., Solomon, S. and Srinivasan, J. 1995. Radiative forcing. In: *Climate change 1994: radiative forcing of climate change and an evaluation of the IPCC IS92 emission scenarios* (eds. J. T. Houghton, L. G. Meira Filho, J. Bruce, H. Lee, B. A. Callander, E. Haites, N. Harris and K. Maskell). Cambridge University Press, Cambridge, 163–204.

Shuttleworth, W. J., Gash, J. H. C., Roberts, J. M., Nobre, C. A., Moline, L. C. B. and Ribeiro, M. D. N. G. 1991. Postdeforestation Amazon climate: Anglo-Brazilian research to improve prediction. *J. Hydrol.* **129**, 71–86.

Stephens, G. L., Randall, D. A., Tjemkes, S. J., Wittmeyer, I. M. and Dazlich, D. A. 1993. The Earth's radiation budget in relation to the hydrologic cycle. Part III. Comparison of observations with a GCM. *J. Geophys. Res.* **98**, 4931–4950.

Suarez, M. J., Arakawa, A. and Randall, D. A. 1983. Parameterization of the planetary boundary layer in the UCLA general circulation model: Formulation and results. *Mon Wea. Rev.* **111**, 2224–2243.

Tans, P. P., Conway, T. J. and Nakazawa, T. 1989. Latitudinal distribution of the sources and sinks of atmospheric carbon dioxide derived from surface observations and an atmospheric transport model. *J. Geophys. Res.* **94**, 5151–5172.

Tans, P. P., Fung, I. Y. and Takahashi, T. 1990. Observational constraints on the global atmospheric CO_2 budget. *Science* **247**,1431–438.

Wofsy, S.C., Harriss, R.C., Kaplan, W.A. 1988. Carbon dioxide in the atmosphere over the Amazon Basin, *J. Geophys. Res.* **93**, 1377–387.

Wofsy, S. C., Goulden, M. L., Munger, J. W., Fan, S.-M., Bakwin, P. S., Daube, B. C., Bassow, S. L. and Bazzaz, F. A. 1993. Net exchange of CO_2 in a mid-latitude forest, *Science* **260**, 1314–316.